# Leukodystrophy resembling Vanishing White Matter Disease is recapitulated by brain-specific depletion of apoptosis regulator MCL-1

**Running title**: MCL-1 is required for white matter integrity

Abigail H. Cleveland[1,2], Alejandra Romero[3], Laurent Alfonso Azcona[2], Melisa Herrero[4], Sheryl Moy[5,6], Orna Elroy-Stein[4,7], Vivian Gama[3,8,9] and Timothy R. Gershon[2,10,11]

[1]UNC Cancer Cell Biology Training Program, University of North Carolina, Chapel Hill, North Carolina 27599, USA

[2]Department of Neurology, UNC School of Medicine, University of North Carolina, Chapel Hill, North Carolina 27599, USA

[3]Vanderbilt University, Cell and Developmental Biology, Nashville, Tennessee 37232, USA .

[4]Shmunis School of Biomedicine and Cancer Research, Faculty of Life Sciences, Tel Aviv University, Tel Aviv, Israel

[5]UNC Carolina Institute for Developmental Disabilities

[6]Department of Psychiatry, UNC School of Medicine, University of North Carolina, Chapel Hill, North Carolina 27599, USA

[7]Sagol School of Neuroscience, Tel Aviv University, Tel Aviv, Israel

[8]Vanderbilt University, Vanderbilt Center for Stem Cell Biology, Nashville, Tennessee 37232, USA .

[9]Vanderbilt University, Vanderbilt Brain Institute, Nashville, Tennessee 37232, USA .

[10]UNC Neuroscience Center, University of North Carolina, Chapel Hill, North Carolina 27599, USA

[11]Lineberger Comprehensive Cancer Center, University of North Carolina, Chapel Hill, North Carolina 27599, USA

**Co-corresponding authors:** Vivian Gama (vivian.gama@vanderbilt.edu) and Timothy R. Gershon (gershont@neurology.med.unc.edu)

## SUMMARY

Diverse mutations cause leukodystrophies through unresolved processes. Developing leukodystrophy therapies requires identifying mechanisms that operate downstream of causative mutations to produce white matter degeneration. We have identified the apoptosis regulator MCL-1 as required for white matter stability and depleted by leukodystrophy-causing mutations. Brain-specific deletion of *Mcl-1* in mice recapitulates progressive leukodystrophy, with MRI changes, decreased oligodendrocytes, and astrocytic and microglial changes typical of Vanishing White Matter Disease (VWMD). Disabling apoptosis through co-deletion of *Bax* or *Bak* rescued white matter *Mcl-1*-dependence, broadly implicating the intrinsic apoptotic pathway in leukodystrophy pathogenesis. *Bax* and *Bak* co-deletions rescued different aspects of the *Mcl-1*-deleted phenotype, demonstrating their discrete roles in white matter stability. MCL-1 protein abundance was reduced in *eif2b5*-mutant mice that model VWMD, suggesting a mechanistic relationship between MCL-1 and VWMD. Our data show that oligodendrocytes require MCL-1 to suppress apoptosis, implicate MCL-1 loss in VWMD pathogenesis, and suggest inhibiting apoptosis for leukodystrophy therapy.

## Introduction

Leukodystrophies are a heterogeneous group of severe neurodegenerative disorders marked by progressive white matter disruption (Raymond, 2017, van der Knaap and Bugiani, 2017). The age of onset varies in each leukodystrophy, but patients typically become symptomatic during childhood, after a latent, asymptomatic period (Kohler et al., 2018, Kohlschutter and Eichler, 2011). Patients with leukodystrophies may experience progressive symptoms including ataxia, dementia,

60 hallucinations, seizures, coma, and death (Vanderver et al., 1993). There is currently
61 no specific targeted therapy that has been clinically implemented to arrest the
62 progression of any leukodystrophy.

63 Diverse pathogenic mutations have been linked to different leukodystrophies
64 (van der Knaap and Bugiani, 2018), but the mechanistic processes through which
65 specific mutations cause white matter degeneration are incompletely understood.
66 Mutations in the apoptotic regulator *APOPT1* (aka *COA8*) cause Progressive
67 Cavitating Leukoencephalopathy, suggesting a role for inappropriate apoptosis in this
68 disease (Melchionda et al., 2014, Yasuda et al., 2006). However, it is not clear why
69 this mutation specifically affects cells of the white matter. Mutations in *eIF2B* subunits
70 result in Vanishing White Matter Disease (VWMD), another leukodystrophy similarly
71 marked by white matter cavitation (Bugiani et al., 2018, van der Knaap et al., 1997,
72 van der Knaap et al., 1993). The causative role of *eIF2B* mutations implicates
73 impaired mRNA translational regulation in VWMD pathogenesis, associated with
74 activation of the Integrated Stress Response (ISR) (van der Knaap et al., 2006, Fogli
75 et al., 2002, Leegwater et al., 2001, Bugiani et al., 2010, Abbink et al., 2019, Kantor
76 et al., 2005). Prior studies have not identified a role for apoptosis in VWMD causation,
77 as seen in Progressive Cavitating Leukoencephalopathy, and whether a common
78 pathogenic process unites these similar phenotypes is unclear.

79 Studies in *eIf2b5* $^{R132H/R132H}$ mice provide insight into the disproportionate effect
80 of *eIF2B* mutations on white matter. These mice develop leukodystrophy resembling
81 VWMD and show impaired mitochondrial function in fibroblasts, astrocytes, and
82 oligodendrocytes (Herrero et al., 2019, Raini et al., 2017, Geva et al., 2010). These
83 studies suggest that *eIF2B* mutations disproportionately affect white matter because
84 glia are more dependent than other types cells on accurate translational regulation

85 and mitochondrial function (Elroy-Stein, 2017). However, several unresolved steps
86 are required to connect the biological processes that have been found to be disrupted
87 in Progressive Cavitating Leukoencephalopathy and VWMD to the observed disease
88 process of progressive leukodystrophy.

89 Identifying proteins that are both required for white matter integrity and
90 affected by *eIF2B* mutations may show specific mechanisms that link VWMD
91 genotype and phenotype. Defining these mechanistic links may show why diverse
92 leukodystrophy mutations produce the final common pathology of white matter
93 degeneration. Identifying proximal mediators of white matter degeneration may also
94 provide important insight into leukodystrophy pathogenesis and treatment.

95 Here we report that mice with conditional deletion of the anti-apoptotic
96 regulator *Mcl-1* targeted to brain stem cells develop progressive postnatal white
97 matter degeneration that recapitulates the phenotype of human leukodystrophies,
98 particularly VWMD. MCL-1 promotes the survival of different cell lineages through its
99 ability to inhibit the pro-apoptotic proteins BAK and BAX, the main effectors of cell
100 death in mammalian cells. Importantly, MCL-1 is a mitochondrial protein that is
101 translationally suppressed by ISR activity (Fritsch et al., 2007), while VWMD disrupts
102 mitochondria and activates the ISR, raising the possibility the MCL-1 deficiency could
103 play a role in the VWMD phenotype.

104 *Mcl-1*-deleted mice were born with normal brain anatomy and show normal
105 motor control and behavior at postnatal day 7 (P7), but then develop increasingly
106 severe ataxia, abnormal motor responses, and extensive white matter atrophy. This
107 white matter-predominant neurodegenerative process closely matches the course of
108 human leukodystrophies with similar postnatal onset of symptoms, MRI changes,
109 progressive white matter degeneration, reduced oligodendrocyte populations,

110 astrocytic abnormalities, and microglial accumulation. Mutations that block the
111 intrinsic apoptotic pathway rescued the phenotype of *Mcl-1* deletion, implicating
112 apoptosis in leukodystrophy pathogenesis, and suggesting a potential approach to
113 therapy.

114

115

116 **Results**

117 **Conditional *Mcl-1* deletion in the CNS causes progressive white matter**
118 **degeneration.**

119 We generated mice with conditional, brain-specific *Mcl-1* deletion by breeding
120 *Mcl-1*$^{loxP/loxP}$ mice that harbor loxP sites around exon 1 of the *Mcl1* locus (Dzhagalov
121 et al., 2007), with *GFAP-Cre* mice that express Cre recombinase in stem cells that
122 give rise to the neurons and glia of the cerebrum and cerebellum, excluding the
123 Purkinje cells (Supp fig. 1A-B) (Zhuo et al., 2001, Kuang et al., 2012). The resulting
124 *hGFAP-Cre/Mcl-1*$^{loxP/loxP}$ (*Mcl-1*$^{cKO}$) mice were born at the expected Mendelian ratio.

125 We compared *Mcl-1*$^{cKO}$ mice to littermate controls, including *Mcl-1*$^{loxP/loxP}$ mice
126 without Cre and heterozygously deleted *hGFAP-Cre/Mcl-1*$^{loxP/+}$. We found no
127 differences between control genotypes and therefore pooled them for analysis.
128 During the first week of life, *Mcl-1*$^{cKO}$ mice showed no deficits and gained weight
129 similarly to controls (Fig. 1A). However, by P14, *Mcl-1*$^{cKO}$ mice showed reduced
130 weight gain (Fig. 1A) and progressive neurologic impairment. While control mice
131 showed normal ability to be weaned at P21, *Mcl-1*$^{cKO}$ mice were unable to be weaned
132 and all died by P23.

133 *Mcl-1*$^{cKO}$ mice demonstrated progressive abnormalities of motor function. We
134 used developmentally adjusted tests to compare behavior of *Mcl-1*$^{cKO}$ mice and
135 controls at P7, P14, and P18. To examine behavior at P7, when mice do not yet have
136 open eyes and do not venture from the nest, we used a test of geotaxis by placing
137 mice on a tilted screen and measuring latency to turn. We also measured latency to
138 turn over in a righting test, and we counted pivots during a 3-min open field test. We
139 found no genotype-specific differences at P7 (Table 1).

140

| Test | WT | *Mcl-1*$^{cKO}$ |
|---|---|---|
| Negative geotaxis (latency, s) | | |
| Trial 1 | 15.4 ± 2 | 14.3 ± 3 |
| Trial 2 | 15.1 ± 2 | 16.7 ± 3 |
| Trial 3 | 15.3 ± 2 | 20.9 ± 3 |
| Righting (latency, s) | 8.2 ± 1 | 10.0 ± 3 |
| Number of pivots | 1.7 ± 0.3 | 1.3 ± 0.5 |

141

142 **Table 1. Neonatal behavior testing showed no effects of *Mcl-1*$^{cKO}$ genotype**
143 **at P7.** Each test was performed on 48 replicate WT pups and 13 replicate *Mcl-*
144 *1*$^{cKO}$ pups at P7. Measures included latency to turn on a tilted screen in a test for
145 geotaxis, and latency to turn over in a righting test. Pivots were counted by an
146 experimenter during a 3-min open field test. One-way ANOVA found no
147 statistically significant differences.

148

149 In contrast to the similar behaviors at P7, by P14 *Mcl-1*$^{cKO}$ mice showed
150 decreased rearing when placed in an open field and spent more time in the center of
151 the open field, while traveling similar distances compared to controls (Fig. 1B; Supp

152 fig. 1C). P18 *Mcl-1*$^{cKO}$ mice also showed a marked increase in limb clasping when
153 vertically suspended (Fig. 1C), a commonly used marker of disease progression in a
154 number of mouse models of neurodegeneration and ataxia (Guyenet et al., 2010,
155 Nakamura et al., 2016).

156 Responses to sensory input were abnormal in *Mcl-1*$^{cKO}$ mice and changed over
157 time. At P14, mice showed increased amplitude of acoustic startle response (Fig. 1D).
158 By P21, when motor function was significantly impaired, the amplitude of acoustic
159 startle response was markedly diminished compared to controls. These data show
160 reduced inhibition in response to sensory stimuli at P14, and reduced motor
161 responses at later ages.

162 Neuropathology studies demonstrated progressive white matter degeneration,
163 that began after the first week of life. At P7, *Mcl-1*$^{cKO}$ brains showed no abnormalities
164 and appeared similar to controls. At P14, *Mcl-1*$^{cKO}$ mice showed white matter
165 rarefaction and ventricular dilation and these changes were more pronounced at P21
166 (Fig. 1E). In addition to white matter loss, we also noted migration abnormalities in
167 the cerebellum, with ectopic cerebellar granule cells in the molecular layer of the
168 cerebellum (Fig. 1E). *Mcl-1*$^{cKO}$ thus showed progressive neuropathology that
169 corresponded temporally with the onset of neurologic symptoms, beginning after P7
170 and increasing over time.

171

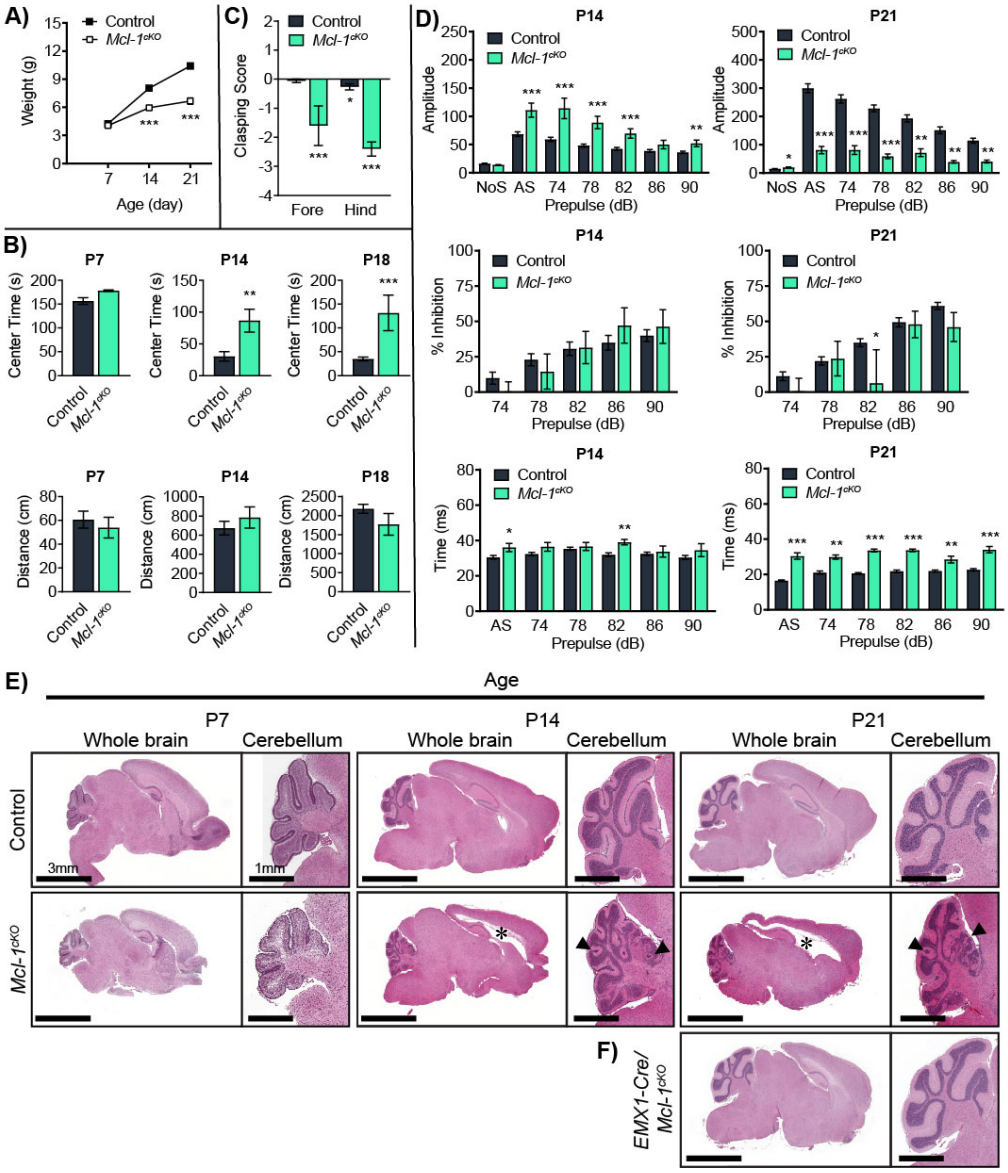


**Figure 1. *Mcl-1* deletion causes progressive motor impairment and white matter degeneration.** (**A**) Reduced weight gain in *Mcl-1*$^{cKO}$ mice compared to controls. (**B**) *Mcl-1*$^{cKO}$ mice show normal motor function at P7, with altered motor function by P14 and (**C**) increased hind-limb clasping at P18. (**D**) *Mcl-1*$^{cKO}$ mice show increased startle in response to auditory stimuli at P14, and reduced elicited movement at P21. (**E**) Brains of representative *Mcl-1*$^{cKO}$ mice shown in H&E-stained sagittal sections appear similar to controls at P7. By P14, *Mcl-1*$^{cKO}$ mice develop white matter degeneration with ventricular enalargment (*) and abnormal migration of cerebellar granule neurons (arrows). White matter loss increases by P21. (**F**) Deleting *Mcl-1* in the neuron-

182 specific *Emx* lineage in *EMX1-Cre/Mcl-1*$^{loxP/loxP}$ mice does not recapitulate the *Mcl-*
183 *1*$^{cKO}$ phenotype. *, ** and *** denote p<0.05, p<0.01 and p<0.001 respectively, relative
184 to controls.

185 **_Mcl-1_ deletion must occur in glia to cause white matter degeneration.**

186 The *GFAP-Cre* transgenic line induces recombination in a broad lineage that
187 includes both glia and neurons (Zhuo et al., 2001). In order to determine whether *Mcl-*
188 *1* loss in neurons drives the *Mcl-1*$^{cKO}$ phenotype, we deleted *Mcl-1* with the neuron-
189 specific *EMX1-Cre* by crossing *Mcl-1*$^{loxP/loxP}$ and *EMX1-Cre* mouse lines. The
190 resulting *EMX1-Cre/Mcl-1*$^{loxP/loxP}$ mice did not develop white matter degeneration or
191 ventriculomegaly (Fig. 1F). In contrast, deletion of *Mcl-1* in *Nestin-Cre/Mcl-1*$^{loxP/loxP}$
192 mice produced white matter degeneration as seen in *Mcl-1*$^{cKO}$ mice (Supp Fig. 2).
193 *Nestin-Cre*, like *GFAP-Cre*, drives recombination in stem cells with neural and glial
194 potential. The phenotype of white matter degeneration thus required *Mcl-1* deletion
195 in the glial lineage.

196 **Blocking apoptosis prevents white matter degeneration in _Mcl-1_-deleted mice**

197 To determine if white matter degeneration in *Mcl-1*$^{cKO}$ mice resulted from
198 increased apoptosis, we examined cell death through cleaved caspase-3
199 immunohistochemistry and TUNEL assays. We did not detect an increase in cleaved
200 caspase-3-stained cells at P7, prior to the onset of white matter loss, or at P14, after
201 white matter loss was evident (data not shown). However, TUNEL staining, performed
202 at P11 when white matter loss was developing, demonstrated increased cell death in
203 *Mcl-1*$^{cKO}$ brains, consistent with a pro-apoptotic effect of *Mcl-1* deletion (Fig. 2A).

204 To determine whether the increased cell death in *Mcl-1*-deleted mice was
205 causally related to the white matter degeneration, we tested whether blocking

206 apoptosis through co-deletion of either *Bax* or *Bak* rescued the *Mcl-1*$^{cKO}$ phenotype.
207 We repeatedly intercrossed *Mcl-1*$^{cKO}$ mice with *Bax*$^{loxP/LoxP}$/*Bak*$^{-/-}$ mice to generate
208 animals with conditional deletion of *Mcl-1* and heterozygous or homozygous deletion
209 of *Bax* or *Bak*. We then raised pups of each genotype and analyzed survival,
210 neurologic function, and neuropathology.

211 We found that co-deletion of *Bax* or *Bak* significantly suppressed the *Mcl-1*$^{cKO}$
212 phenotype, but resulted in different, mitigated phenotypes. *Mcl-1*-deleted mice with
213 heterozygous co-deletion of *Bak*, with the genotype *hGFAP-Cre/Mcl1*$^{loxP/loxP}$/*Bak*$^{-/+}$
214 (*Mcl-1*$^{cKO}$/*Bak*$^{-/+}$), showed normal survival without overt neurologic deficits and normal
215 white matter and cerebellar migration (Fig. 2B). In contrast, *Mcl-1*-deleted mice with
216 heterozygous co-deletion of *Bax*, with the genotype *hGFAP-Cre/Mcl1*$^{loxP/loxP}$/*Bax*$^{loxP/+}$
217 (*Mcl-1*$^{cKO}$/*Bax*$^{fl/+}$), showed a progressive leukoencephalopathy phenotype similar *Mcl-*
218 *1*$^{cKO}$ mice (Fig. 2B). Immunohistochemistry demonstrated markedly lower BAK
219 protein in *Bak*$^{+/-}$ animals (Fig. 2C), indicating that that heterozygous *Bak* deletion was
220 sufficient to alter BAK expression. The rescued phenotype of *Mcl-1*$^{cKO}$/*Bak*$^{-/+}$ mice
221 therefore demonstrated reducing BAK protein expression was sufficient to prevent
222 white matter degeneration.

223

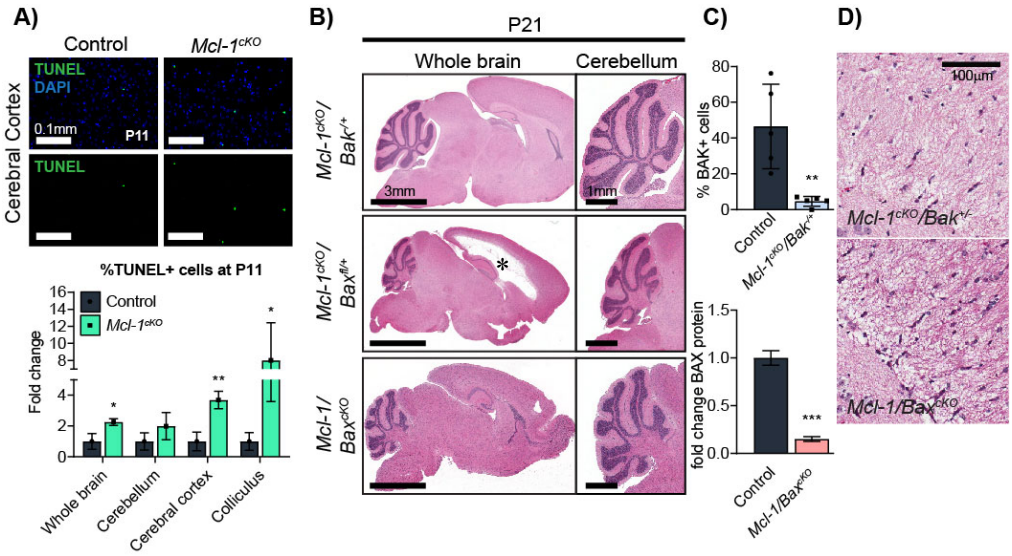


**Figure 2. *Mcl-1* deletion causes white matter degeneration by increasing apoptosis.** (**A**) TUNEL demonstrates increased cell death in *Mcl-1*$^{cKO}$ brains. For cell counts, one sagittal section from each replicate was scanned at 20x and TUNEL+ cells were counted across the entire portion of each designated region that was contained within the section. (**B**) Representative H&E sections show that heterozygous *Bak* co-deletion and homozygous *Bax* co-deletion both rescue the white matter loss with ventricular enlargement (*) and cerebellar abnormalities caused by *Mcl-1* deletion. (**C**) Quantification of BAK immunohistochemistry in corpus callosum shows that heterozygous *Bak* deletion significantly reduces the number of BAK+ cells. Quantification of western blot of whole cerebella shows that homozygous *Bax* deletion reduces BAX protein abundance. (**D**) Representative images of the corpus callosum in P14 mice of the indicated genotypes shows mild white matter rarefaction in *Mcl-1/Bax*$^{dKO}$ mice, not seen in *Mcl-1*$^{cKO}$*/Bak*$^{+/-}$ mice. *, ** and *** denote $p<0.05$, $p<0.01$ and $p<0.001$ respectively, relative to controls.

*Mcl-1*-deleted mice with homozygous *Bax* co-deletion, with the genotype *hGFAP-Cre/Mcl1*$^{loxP/loxP}$*/Bax*$^{loxP/loxP}$ (*Mcl-1/Bax*$^{dKO}$) showed normal survival, similar to *Mcl-1*$^{cKO}$*/Bak*$^{-/+}$ mice. Compared to *Mcl-1*$^{cKO}$ mice, *Mcl-1/Bax*$^{dKO}$ mice showed greatly reduced neurologic deficits; however, we noted that by 200 days, *Mcl-1/Bax*$^{dKO}$ showed a slight delay in movement on opening the cage that was not seen in *Mcl-*

244 *1$^{cKO}$/Bak$^{+/-}$* mice. The extensive white matter loss in *Mcl-1$^{cKO}$* mice was rescued in
245 *Mcl-1/Bax$^{dKO}$* mice (Fig. 2B). Close examination of brain sections from *Mcl-1/Bax$^{dKO}$*
246 mice, however, showed mild white matter loss (Fig 2D). The rescued phenotypes of
247 *Mcl-1$^{cKO}$/Bak$^{-/+}$* and *Mcl-1/Bax$^{dKO}$* mice show that disrupting either *Bax* or *Bak* is
248 sufficient to prevent the severe white matter degeneration that otherwise results from
249 *Mcl-1* deletion, implicating apoptosis in the pathogenesis of the *Mcl-1$^{cKO}$* phenotype.
250 The mild neurologic deficits and white matter loss in *Mcl-1/Bax$^{dKO}$* mice showed that
251 co-deletion of *Bax* and *Bak* do not have identical effects in *Mcl-1*-deleted animals.

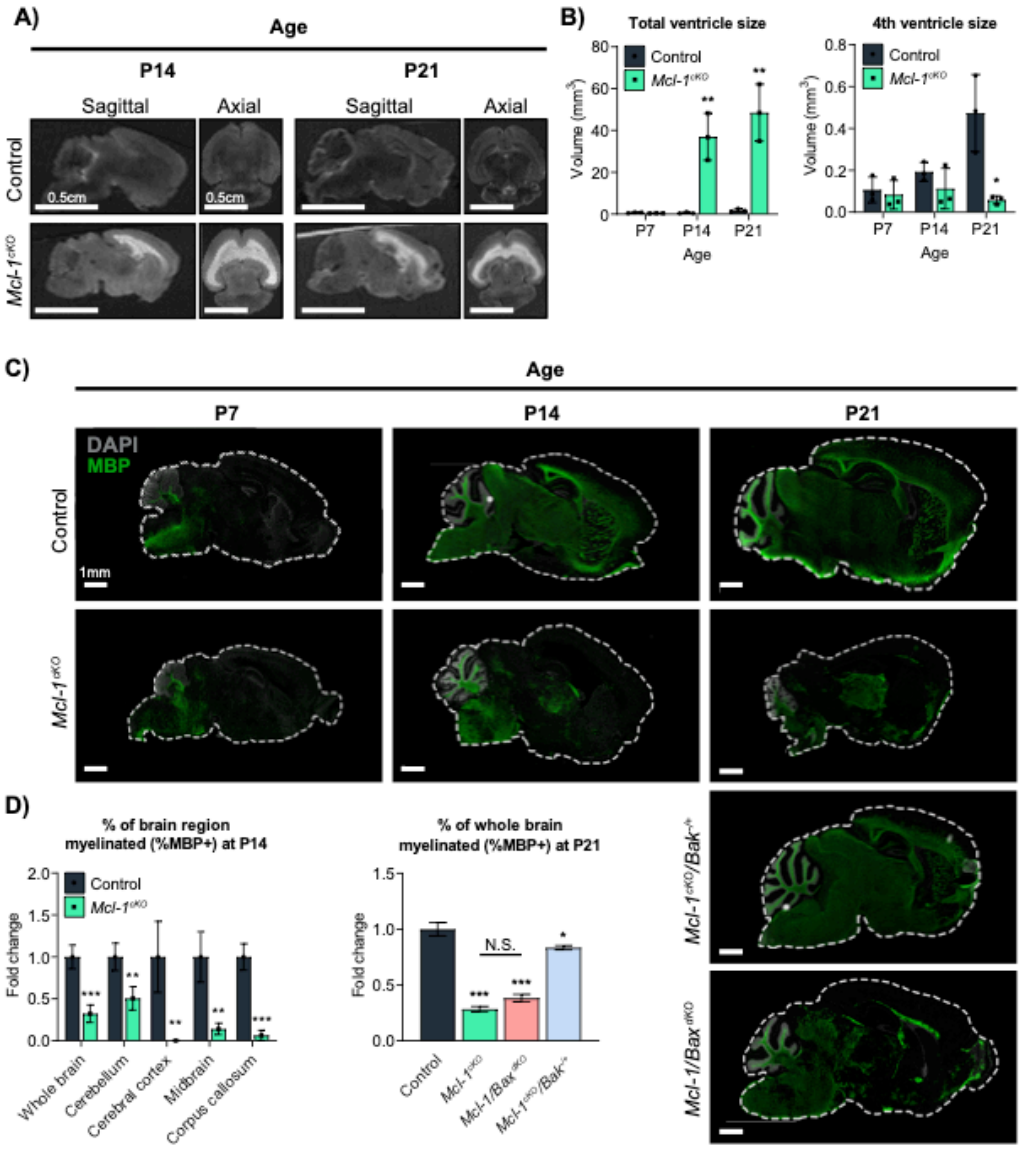


252

253 **Figure 3. Abnormal neuroimaging and myelination in *Mcl-1*-deleted mice, with**
254 **different rescue effects caused by co-deletion of *Bak* or *Bax*.** (**A**) Representative
255 MRIs show white matter hyperintensity in *Mcl-1*$^{cKO}$ mice. (**B**) Total ventricular volume
256 is abnormal in *Mcl-1*$^{cKO}$ mice and increases from P7-P21, while the volume of the 4$^{th}$
257 ventricle decreases significantly by P21. (**C,D**) Representative images and
258 quantitative analysis of MBP IHC show that myelination is markedly decreased in *Mcl-*
259 *1*$^{cKO}$ mice, rescued in *Mcl-1*$^{cKO}$*/Bak*$^{+/-}$ mice, and incompletely rescued in *Mcl-1/Bax*$^{dKO}$

260 mice. **(D)** Graphs show MBP+ area/total area within individual sections, normalized
261 to the mean value in the control mice. *, ** and *** denote $p<0.05$, $p<0.01$ and
262 $p<0.001$ respectively, relative to controls.

263 **Mcl-1 deletion phenocopies human leukodystrophies**

264 Leukoencephalopathies in patients produce characteristic MRI findings,
265 including high water signal in white matter tracts (Vanderver et al., 1993), and the
266 replacement of white matter by cerebrospinal fluid (van der Knaap et al., 1993). We
267 analyzed whether *Mcl-1*$^{cKO}$ mice showed similar white matter changes on MRI. Similar
268 to VWMD patients, *Mcl-1*$^{cKO}$ mice showed progressive ventriculomegaly (Fig. 3A).
269 The increase in ventricle size was not evenly distributed, however, as the volume of
270 the 4$^{th}$ ventricle was significantly smaller in *Mcl-1*$^{cKO}$ mice at P21 (Fig. 3B). Increased
271 lateral ventricles and reduced 4$^{th}$ ventricle was consistent with loss of periventricular
272 cerebral white matter and an overall reduction in intracranial pressure, indicating
273 hydrocephalus *ex vacuo*.

274 To determine whether myelination was disrupted in *Mcl-1*$^{cKO}$ mice, we
275 analyzed the distribution of Myelin Basic Protein (MBP). In control brains, the MBP+
276 area increased markedly from P7 to P14 (Fig 3C). In contrast, myelination was
277 delayed in *Mcl-1*$^{cKO}$ brains, which showed significantly less MBP+ area at P14 in all
278 brain regions analyzed (Fig. 3D).

279 Analysis of MBP+ area in *Mcl-1*-deleted mice with *Bax* or *Bak* co-deletions
280 showed that myelination required MCL-1 specifically to regulate BAK. We compared
281 brains in P21 animals, when normal brains show widespread myelination.
282 Heterozygous *Bak* co-deletion largely rescued myelination in *Mcl-1*$^{cKO}$*/Bak*$^{+/-}$ mice. In
283 these animals, MBP+ area was over 2-fold greater than in *Mcl-1*$^{cKO}$ mice, although

284 we noted a small, statistically significant decrease in myelination compared to *Mcl-1*
285 intact controls. Homozygous *Bax* deletion, however, did not rescue myelination in
286 *Mcl-1/Bax*$^{dKO}$ mice (Fig. 3D). The differential effects of *Bak* or *Bax* deletion on
287 myelination support the interpretation that BAX and BAK act in cells with different
288 functions, with both BAX and BAK affecting white matter maintenance, and only BAK
289 affecting myelination.

290

291 ***Mcl-1* deletion reduces oligodendrocyte and Bergmann glia populations**

292 To determine if impaired myelination in *Mcl-1*$^{cKO}$ mice resulted from
293 oligodendrocyte loss, we compared the numbers of cells expressing the
294 oligodendrocyte marker SOX10 in *Mcl-1*$^{cKO}$ and control mice (Fig. 4A). SOX10 marks
295 the oligodendrocyte lineage from the initial fate commitment in oligodendrocyte
296 precursors to the maturation of myelinating oligodendrocytes (Glasgow et al., 2014,
297 Nishiyama et al., 2016); SOX10 cell counts thus reflect the total oligodendrocytic
298 population across the differentiation spectrum. At P7, oligodendrocyte populations in
299 *Mcl-1*$^{cKO}$ mice were not significantly different from controls. By P14, *Mcl-1*$^{cKO}$ mice
300 showed significantly fewer SOX10+ cells in diverse brain regions (Fig. 4B), indicating
301 a global decrease in oligodendrocytic cells. At P21, oligodendrocytic populations
302 remained reduced in the cerebellum, corpus callosum, and superior colliculus, but
303 were not statistically significantly reduced in the hippocampus and cerebral cortex,
304 raising the possibility of a dynamic, homeostatic response in these gray matter
305 regions.

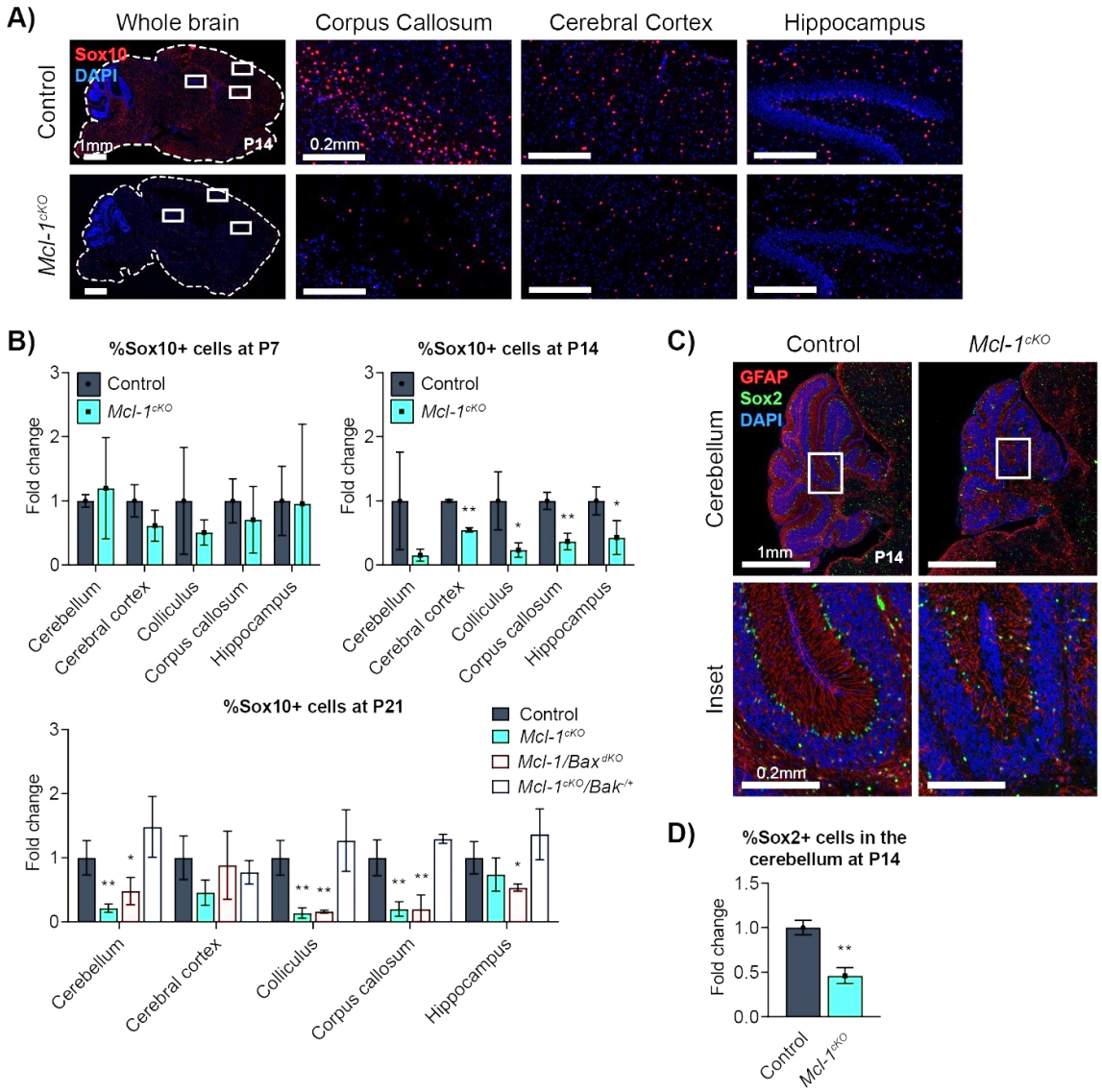


**Figure 4. *Mcl-1* deletion causes loss of oligodendrocytes and Bergmann glia that is rescued with regional variation by co-deletion of *Bak* or *Bax*.** (**A,B**) Representative images and quantification of SOX10 IHC in the indicated genotypes. (**C**) Representative immunofluorescence for GFAP and SOX2 IHC identify Bergmann glia in P14 mice of indicated genotypes. (**D**) SOX2+ cells are significantly reduced in *Mcl-1*$^{cKO}$ mice. * and ** denote $p<0.05$ and $p<0.01$ respectively, relative to controls.

To determine if apoptosis mediates the decline in the oligodendrocyte populations in *Mcl-1*-deleted mice, we examined the effect of *Bax* or *Bak* co-deletion in *Mcl-1*$^{cKO}$*/Bak*$^{+/-}$and *Mcl-1/Bax*$^{dKO}$ mice. Heterozygous *Bak* co-deletion in *Mcl-*

316 *1$^{cKO}$/Bak$^{+/-}$* mice normalized oligodendrocyte population size, but homozygous *Bax*
317 deletion in *Mcl-1/Bax$^{cKO}$* mice did not (Fig. 4B). *Bak* co-deletion thus rescued the
318 effects of *Mcl-1* deletion on white matter volume, myelination, and total
319 oligodendrocyte populations. In contrast, *Bax* co-deletion rescued only white matter
320 volume, but myelination and oligodendrocyte numbers remained affected in *Mcl-*
321 *1/Bax$^{dKO}$* mice. The discordant effects of *Bak* and *Bax* co-deletions suggest that MCL-
322 1 discretely controls BAK-dependent apoptosis or BAX-dependent apoptosis in
323 different types of white matter cells.

324 In contrast to the discordant effects of *Bax* and *Bak* co-deletions in
325 oligodendrocytes, Bergmann glia were rescued by either co-deletion. We examined
326 Bergmann glia because of their known involvement in VWMD (Dooves et al., 2016),
327 and because of the migration abnormalities in *Mcl-1$^{cKO}$* mice, as Bergmann glia guide
328 cerebellar granule neuron progenitors as they migrate to the internal granule cell layer
329 to become cerebellar granule neurons (Hatten, 1990, Rakic, 1971). We identified
330 Bergmann glia as cells with SOX2+ nuclei and GFAP+ processes (Fig. 4C). At P7,
331 the numbers of Bergmann glia in *Mcl-1$^{cKO}$* were similar to control mice (data not
332 shown), but by P14, the Bergmann glia populations in *Mcl-1$^{cKO}$* mice were significantly
333 reduced (Fig. 4D). The loss of Bergmann glia during the period of CGN migration
334 account for the observed cerebellar migration defects. Co-deletion of either one copy
335 of *Bak* in *Mcl-1$^{cKO}$/Bak$^{+/-}$* mice or both copies of *Bax* in *Mcl-1/Bax$^{dKO}$* mice was
336 sufficient to rescue cerebellar migration, indicating that MCL-1 functions in Bergmann
337 glia to restrict an apoptotic program that requires both BAX AND BAK in order to drive
338 cell death.

339

340

341 ***Mcl-1* deletion alters the astrocytic populations**

342 While *Mcl-1*$^{cKO}$ mice contained fewer Bergmann glia, we noted increased
343 numbers of GFAP+ astrocytic processes throughout the brain, that was most
344 conspicuous in the relatively hypocellular molecular layer of the cerebellum (Fig. 5A).
345 To determine if this increase in GFAP+ cells indicated an increase in the total number
346 of astrocytes or an increase in the fraction of astrocytes expressing GFAP, we
347 compared the number of cells expressing the astrocytic nuclear marker SOX9 in *Mcl-*
348 *1*$^{cKO}$ mice and controls (Fig. 5B). SOX9+ cells were not significantly increased in *Mcl-*
349 *1*$^{cKO}$ mice in any brain region at either P7 or P14, and rather were decreased in the
350 corpus callosum at P14 (Fig. 5B,C). The increase in GFAP+ processes in *Mcl-1*$^{cKO}$
351 mice without the increase in SOX9+ cells shows the *Mcl-1* deletion did not increase
352 the total astrocyte population, but rather increased the fraction of astrocytes
353 expressing GFAP, indicating a reactive response to injury (Eddleston and Mucke,
354 1993, Dahl and Bignami, 1974).

355 The intermediate filament protein NESTIN is known to be up-regulated in
356 reactive astrocytes (Tamagno and Schiffer, 2006, Schmidt-Kastner et al., 2005, Sahin
357 Kaya et al., 1999, Clarke et al., 1994), and prior studies report increased Nestin-
358 expressing astrocytes in white matter from humans with VWMD (Bugiani et al., 2011).
359 Similarly, *eIF2B5* $^{R191H/R191H}$ mice show increased astrocytes expressing both Nestin
360 and GFAP in the corpus callosum, compared to wildtype controls (Dooves et al.,
361 2016, Geva et al., 2010). To determine if *Mcl1*-deleted mice also showed similar
362 astrocytic changes, we compared Nestin+/GFAP+ populations in P14 *Mcl-1*$^{cKO}$ mice
363 and controls (Fig. 5D). *Mcl-1*$^{cKO}$ mice demonstrated increased fractions of

364 Nestin+/GFAP+ cells in the corpus callosum (Fig 5E), with a trend toward increased
365 fractions in other white matter regions, consistent with astrocytic changes in VWMD
366 patients and *eIF2B5* $^{R191H/R191H}$ mice. *Mcl-1*$^{cKO}$ mice thus recapitulated both the
367 astrocytic and oligodendrocytic abnormalities seen in VWMD in patients and the
368 VWMD mouse models.

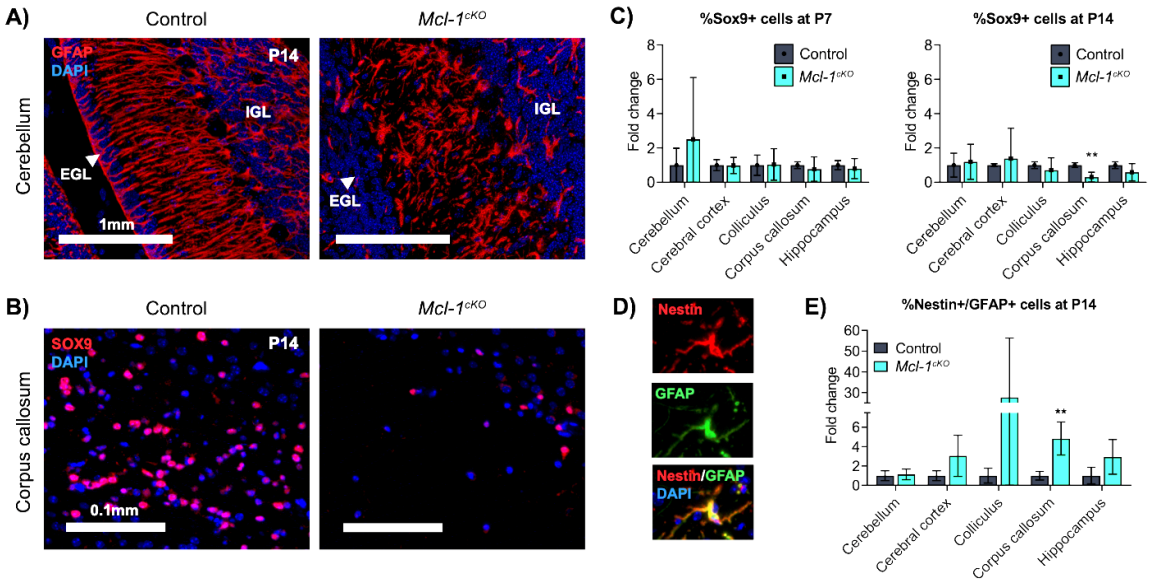


369

370 **Figure 5. Mcl-1 deletion causes reactive astrocytosis.** (**A**) Representative GFAP
371 IHC in sections of P14 cerebella in the indicated genotypes shows Bergmann glia
372 processes in the control mice that are absent in the *Mcl-1*$^{cKO}$, and numerous astrocyte
373 processes in the *Mcl-1*$^{cKO}$ mice. (**B**) Representative SOX9 IHC in sections of P14
374 corpus callosum in the indicated genotypes show a significant decrease of SOX9+
375 cells in the *Mcl-1*$^{cKO}$ mice. (**C**) Quantification of SOX9 IHC at the indicated ages and
376 genotypes, showing that astrocyte numbers are not increased in *Mcl-1*$^{cKO}$ mice. (**D,E**)
377 Nestin/GFAP IHC, with representative images and quantification in the indicated
378 genotypes. * and ** denote $p<0.05$ and $p<0.01$ respectively, relative to controls.

379 **Mcl-1 deletion causes neuroinflammation**

380 Brains of *Mcl-1*$^{cKO}$ mice contained increased cells expressing the myeloid
381 marker IBA1 (Fig. 6A), indicating microglial activation (Ito et al., 1998, Imai et al.,

382 1996). The microglial changes in *Mcl-1*$^{cKO}$ mice began later than the astrocytic and
383 oligodendrocytic changes, beginning at the corpus callosum at P14; by P21, *Mcl-1*$^{cKO}$
384 mice showed increased IBA+ cells in diverse brain regions (Fig. 6B). The increased
385 IBA1+ microglia in *Mcl-1*$^{cKO}$ mice demonstrates a non-cell autonomous effect in which
386 *Mcl-1* deletion in the glio-neuronally restricted GFAP lineage induced inflammatory
387 changes in myeloid cells.

388 Co-deletion of either *Bak* or *Bax* prevented microgliosis in different brain
389 regions. Heterozygous co-deletion of *Bak* in *Mcl-1*$^{cKO}$*; Bak*$^{+/-}$ mice significantly
390 reduced IBA1+ cells in the cerebellum, cerebral cortex, colliculus, and corpus
391 callosum, relative to *Mcl-1*$^{cKO}$ mice. In contrast, homozygous co-deletion of *Bax* in
392 *Mcl-1*$^{/}$*Bax*$^{dKO}$ mice showed a significant decrease in IBA1+ cells in the hippocampus,
393 relative to both *Mcl-1*$^{cKO}$ and *Mcl-1*$^{cKO}$*/Bak*$^{+/-}$ mice (Fig. 6B). The rescue of neuro-
394 inflammation by co-deletion of *Bax* or *Bak* implicates increased regional apoptosis as
395 the cause of inflammation, while the region-specific pattern of rescue further supports
396 the conclusion that white matter cells in different areas of the brain alternatively
397 regulate apoptosis through interactions of MCL-1 with either BAX or BAK.

398 **Decreased brain MCL-1 protein in a VWMD mouse model**

399 Based on the similarity of the *Mcl-1*$^{cKO}$ phenotype to VWMD, the role of the ISR in
400 VWMD, and the regulation of MCL-1 abundance by the ISR, we investigated whether
401 changes in MCL-1 protein might mediate the effect of mutant eIF2B on glial cells. To
402 begin to test this possibility, we compared MCL-1 abundance in brain lysates from
403 wildtype and *eIF2B5* $^{R132H/R132H}$ mice at 7 and 10 months old (Fig. 6C). We found that
404 by 10 months, *eIF2B5* $^{R132H/R132H}$ mice expressed reduced MCL-1 protein in the brain,
405 indicating that the *eIF2B5* $^{R132H/R132H}$ mutation results in reduced MCL-1 expression

406 over time. In *eIF2B5* $^{R132H/R132H}$ mice, the temporal course of reduced brain MCL-1
407 protein correlated with the development of VWMD symptoms. Thus, along with our
408 finding that MCL-1 deficiency in *Mcl-1*$^{cKO}$ mice was sufficient to cause a VWMD
409 phenotype, we found declining MCL-1 expression in *eIF2B5* $^{R132H/R132H}$ mice that
410 model VWMD.

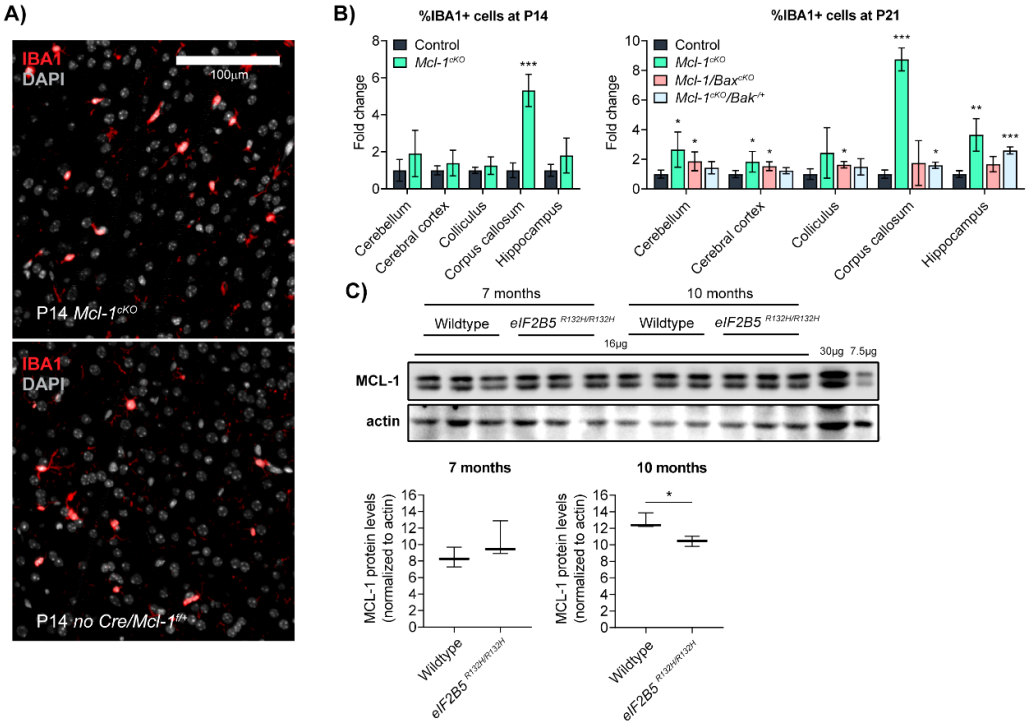


411

412 **Figure 6. Progressive neuroinflammation in *Mcl-1*$^{cKO}$ mice and reduced MCL-1**
413 **protein in mice with VWMD.** (**A,B**) IBA1 IHC, with representative images and
414 quantification in the indicated genotypes, showing a progressive increase in microglia
415 in *Mcl-1*$^{cKO}$ mice, beginning in the corpus callosum at P14 and expanding to include
416 diverse regions by P21. Co-deletion of *Bak* or *Bax* variably rescue microgliosis with
417 different effects in different regions. *, ** and *** denote p<0.05, p<0.01 and p<0.001
418 respectively, relative to controls. (**C**) Western blot comparing MCL-1 protein
419 abundance in brain lysates of 7- and 10-months old WT and *eIF2B5*$^{R132H/R132H}$ mice,
420 demonstrating reduced MCL-1 in 10-month old mutant mice. * denotes p<0.03,
421 relative to controls.

422 **Discussion**

423 Our data show that conditional deletion of anti-apoptotic *Mcl-1* in neuro-glial
424 stem cells results in a progressive encephalopathy with post-natal white matter
425 degeneration. While prior studies have shown increased apoptosis in embryonic and
426 adult neural progenitors resulting from *Mcl-1* deletion (Fogarty et al., 2019, Hasan et
427 al., 2013, Malone et al., 2012), our data show that the predominant effect of *Mcl-1*
428 deletion in the postnatal brain is white matter degeneration. Although MCL-1
429 mutations have not been described in any human leukodystrophy, the mechanisms
430 of white matter injury in human leukodystrophies are unresolved. Our studies show
431 that altered MCL-1-dependent regulation of apoptosis can drive the pathogenesis of
432 leukodystrophy.

433 The *Mcl-1*$^{cKO}$ phenotype presented striking similarities to human
434 leukodystrophies, and most specifically to VWMD. Brain function and white matter
435 appeared normal in *Mcl-1*$^{cKO}$ mice until after P7, when mice showed motor and
436 sensory impairment, delayed myelination, and rarefaction of the periventricular white
437 matter and corpus callosum, eventually leading to white matter loss and
438 hydrocephalus *ex vacuo*. Similar to VWMD, mature myelinating oligodendrocytes
439 were markedly reduced, Bergmann glia of the cerebellum were also affected, and
440 astrocytes showed reactive changes that are also seen in astrocytes in VWMD,
441 including up-regulation of GFAP and NESTIN. The similarity of the *Mcl-1*$^{cKO}$ and
442 VWMD phenotypes, including the overall histopathology of vanishing white matter
443 and the specific loss of terminally differentiated oligodendrocytes and Bergmann glia,
444 show that *eIF2B* mutations and *Mcl-1* deletion affect specific cells of the brain in a
445 similar manner.

446 Taken together, reduced MBP and SOX10 demonstrate that within global
447 oligodendrocyte depletion of *Mcl-1*$^{cKO}$ mice, mature, myelinating oligodendrocytes are
448 particularly affected. Studies in VWMD patients and mouse models show that while
449 mature oligodendrocyte populations are reduced, immature oligodendrocyte
450 precursors may actually be increased (Herrero et al., 2019, Bugiani et al., 2013). A
451 similar increase in immature oligodendrocytes may occur in the *Mcl-1*$^{cKO}$ mice and
452 would not be inconsistent with the observed overall reductions in SOX10+ brain cells
453 and brain myelination.

454 The similarity of the *Mcl-1*$^{cKO}$ phenotype to VWMD raises the possibility that
455 reduced MCL-1 protein abundance specifically contributes to VWMD pathology. The
456 known activation of the ISR in VWMD (Abbink et al., 2019, Kantor et al., 2005) and
457 the suppression of MCL-1 translation by the ISR together provide a potential
458 molecular mechanism to link the *Mcl-1*$^{cKO}$ phenotype to VWMD. Consistent with this
459 proposed mechanism, we found reduced MCL-1 protein in *eIF2B5* $^{R132H/R132H}$ mice,
460 which correlated with the development of white matter pathology. While studies in
461 patient-derived samples could potentially test whether MCL-1 abundance is altered
462 in VWMD patients, these studies would require samples that preceded fulminant
463 white matter loss, in order to include oligodendrocyte populations that may be lost
464 through apoptosis. Our data show that MCL-1 deficiency is sufficient to reproduce the
465 VWMD phenotype in mice. Studies of *Bax* and *Bak* deletion in *eIF2B5* $^{R132H/R132H}$ mice
466 would allow testing of whether apoptosis is required for VWMD.

467 The rescue of the *Mcl-1*$^{cKO}$ phenotype by co-deletion of *Bak* or *Bax* implicate
468 apoptosis in the causation of white matter loss in *Mcl-1*$^{cKO}$ mice. We previously found
469 that conditional *Mcl-1* deletion in cerebellar granule neuron progenitors does not

470 produce a phenotype of gray matter loss as these cells regulate BAX via the
471 homologous anti-apoptotic protein BCL-xL *(Crowther et al., 2013)*. The specific
472 dependencies of different cell types on different anti-apoptotic factors is also seen
473 outside the nervous system, as in the myeloid lineage where neutrophils undergo
474 spontaneous apoptosis when *Mcl-1* is deleted, but macrophages survive (Dzhagalov
475 et al., 2007). Different cell types within broad lineages may thus require different anti-
476 apoptotic family proteins to regulate apoptosis, and the survival of neurons and
477 astrocytes in *Mcl-1*$^{cKO}$ mice shows that within the broad lineage derived from glio-
478 neuronal stem cells, MCL-1 protein is specifically required by a subset of cells at some
479 point along the more narrow lineage of the oligodendrocytes.

480 In addition to demonstrating the requirement for apoptosis in white matter
481 degeneration in *Mcl-1*$^{cKO}$ mice, the *Bax* and *Bak* rescue studies demonstrate that
482 myelination defects and white matter loss can be dissociated. Co-deletion of *Bak*
483 rescued both myelination, oligodendrocyte populations, and white matter loss. In
484 contrast co-deletion of *Bax* reduced white matter loss without rescuing myelination
485 and oligodendrocyte populations. These differences show that different cell types that
486 can be differentiated by their apoptosis regulation contribute to different aspects of
487 the *Mcl-1*$^{cKO}$ phenotype.

488 The possibility that BAX and BAK act in different cells with different sensitivities
489 does not require differential expression patterns. For example, prior studies show that
490 both BAX and BAK can drive apoptosis in cerebellar granule neuron progenitors, but
491 under different conditions. BAX-dependent apoptosis in these cells can be engaged
492 either by radiation-induced DNA damage (Chong et al., 2000), or by chromosomal
493 fragmentation in the setting of *Atr* deletion (Lang et al., 2016). In contrast, BAK-

494 dependent apoptosis is not engaged by radiation, as radiation induced apoptosis is
495 blocked by *Bax* deletion(Crowther et al., 2013, Chong et al., 2000); BAK-dependent
496 apoptosis requires the more intense trigger of *Atr* deletion and resulting chromosomal
497 fragmentation (Lang et al., 2016). These prior studies show that cells in the CNS that
498 express both BAX and BAK can show different mechanisms and sensitivities for
499 triggering BAX-dependent or BAK-dependent apoptosis. Similarly, specific subsets of
500 glia may regulate BAX-dependent and BAK-dependent apoptosis through different
501 mechanisms, with different, cell-type specific sensitivities and dependencies on MCL-
502 1.

503 The rescue myelination by co-deletion of *Bak* but not *Bax* shows that
504 myelinating oligodendrocytes or their precursors regulate apoptosis specifically
505 through MCL-1:BAK interactions. The different rescue pattern with *Bax* co-deletion,
506 which prevented white matter degeneration without normalizing myelination, shows
507 that a different type of cell regulates white matter loss and requires both BAK and
508 BAX to be present for *Mcl-1* deletion to produce phenotype changes. Clearly, diverse
509 cell types are affected in both *Mcl-1*$^{cKO}$ mice and VWMD patients (Bugiani et al., 2018,
510 Zhou et al., 2019). Our genetic rescue studies show that different types of glial cells
511 depend on MCL-1 to regulate different pro-apoptotic proteins, and that loss of this
512 regulation in different types of cells reproduces different aspects of the overall
513 pathology. The loss of multiple subsets of glial cells may similarly contribute to
514 different aspects of the overall VWMD phenotype.

515 While multiple mutations can cause leukodystrophies, for many of these
516 genetic diseases, the mechanistic steps from mutation to white matter loss remain to
517 be specified in detail. Our findings that MCL-1 deletion in neuro-glial stem cells

518 produces white matter degeneration, and that this degeneration is rescued by co-
519 deletion of *Bax* or *Bak* implicates the process of apoptosis in the causation of
520 leukodystrophy. Moreover, our rescue experiments show that apoptosis in multiple
521 cell types derived from neuro-glial stem cells contribute to different aspects of white
522 matter pathology. Treatments that inhibit the intrinsic apoptotic pathway in the
523 postnatal brain may provide an avenue for reducing the impact of diverse
524 leukodystrophies.

525

526 **Acknowledgments:** supported by R01NS088219 (TRG), R01NS102627 (TRG), and
527 R01NS1062 (TRG), T32CA071341 (AHG), 4R00CA178190 (VG), R35GM128915
528 (VG), and R21CA227483 (VG).
529

530 **Author Contributions**: Conceptualization, T.R.G. and V.G.; Methodology, A.H.C.,
531 T.R.G., V.G. and O.E-S.; Investigation, A.H.C, A.R., L.A.A., M.H.,; Writing – Original
532 Draft, A.H.C. and T.R.G.; Writing – Review & Editing, O.E-S., V.G. and T.R.G;
533 Funding Acquisition, V.G., and T.R.G.;; Resources, O.E-S., V.G., and T.R.G.;
534 Supervision, O.E-S., V.G., and T.R.G.

535

536 **Methods**

537 **Mice**

538 We generated *Mcl-1*$^{cKO}$ mice, by crossing *GFAP-Cre* mice (Jackson Labs, stock #
539 004600) with *Mcl-1*$^{LoxP/LoxP}$ mice (Dzhagalov et al., 2007), generously shared by Dr.
540 You-Wen He. We interbred GFAP-Cre, *Mcl-1*$^{loxP/loxP}$, and *Bax*$^{LoxP/LoxP}$*/Bak*$^{-/-}$ (Jackson
541 Labs, stock # 006329) to generate *Mcl-1;Bax*$^{dKO}$, *Mcl-1;Bak*$^{dKO}$, and various
542 heterozygous controls. We generated *EMX1-Cre/Mcl-1*$^{loxP/loxP}$ mice by breeding
543 *EMX1-Cre* mice, generously provided by Dr. William Snide, into the *Mcl-1 f/f* line. All
544 mice were of species *Mus musculus* and crossed into the C57BL/6 background

545 through at least five generations. All animal studies were carried out with the approval
546 of the University of North Carolina Institutional Animal Care and Use Committee
547 under protocols (19-099).

548 Wild type (C57BL/6 strain) and *eIF2B5*$^{R132H/R132H}$ mice (Geva et al., 2010) were
549 generated, bred, and housed in Tel Aviv University animal facility (Lab Products Inc.,
550 Seaford, DE, USA). All experimental procedures were approved by the Tel Aviv
551 University Animal Care Committee according to national guidelines (permit #04-17-
552 022). Breeding and genotyping were performed as previously described. (Geva et al.,
553 2010) Each generation was established by back cross of homozygous
554 *eIF2B5*$^{R132H/R132H}$ mice with WT C57BL/6J (Harlan Labs, Jerusalem, Israel) to prevent
555 genetic drift.

556

557 **Histology and immunohistochemistry (IHC)**

558 Mouse brains were processed and immunostained as previously described (Ocasio
559 et al., 2019, Tech et al., 2017, Lang et al., 2016, Crowther et al., 2016). Primary
560 antibodies used were: BAK diluted 1:200 (Cell Signaling, #12105), MBP diluted
561 1:1000 (Abcam, #ab7349), SOX10 diluted 1:100 (Santa Cruz, #sc-17342), cleaved-
562 Caspase 3 (cC3) diluted 1:400 (Biocare Medical, #CP229C), glial fibrillary acidic
563 protein (GFAP) diluted 1:2000 (Dako, Z0334), SOX2 1:200 (Cell Signaling, #4900S),
564 SOX9 1:200 (R&D Systems, #AF3075), NESTIN 1:500 (Cell Signaling, #4760), IBA1
565 1:2000 (Wako Chemicals, #019-19741). Stained images were counterstained with
566 DAPI, digitally imaged using an Aperio Scan Scope XT (Aperio) and subjected to
567 automated cell counting using Tissue Studio (Definiens).

568

569 **Magnetic resonance imaging**

570 For MRI studies, brains from P7, P14, and P21 mice were harvested and fixed in 4%
571 formaldehyde in PBS for 48hrs, then transferred to PBS. Brains were then embedded
572 in 2% agarose in 15mL plastic vials and imaged in pairs as previously described
573 (Williams et al., 2015).
574
575 **Western blot**
576 Whole brains or cerebella were harvested and homogenized in lysis buffer (Cell
577 Signaling, #9803). Lysate protein concentrations were quantified using a
578 bicinchoninic acid (BCA) protein assay kit (Thermo scientific, #23225). Equal total
579 protein concentrations were resolved on SDS-polyacrylamide gels (BioRad, #
580 4561105, # 4568094) and transferred onto polyvinylidene difluoride membranes.
581 Membranes were blotted using a SNAP i.d. 2.0 Protein Detection System (Millipore).
582 Membranes were imaged using a chemiluminescent SuperSignal West Femto
583 Maximum Sensitivity Substrate (34095, Thermo Fisher Scientific) and the C-DiGit blot
584 scanner (LI-COR Biosciences). Signal was quantified using the Image Studio Lite
585 software (LI-COR). The following antibodies were used for western blot: MCL-1 (Cell
586 Signaling, #94296; 1:500 dilution), BAX (Cell Signaling, #14796; 1:500 dilution), β-
587 actin (Cell Signaling, #3700; 1:5000 dilution), Actin (Sigma #A3853; 1:240000
588 dilution), Anti-rabbit IgG, HRP-linked antibody (Cell Signaling, #7074; 1.5:1000
589 dilution), Anti-mouse IgG, HRP-linked antibody (Cell Signaling, #7076; 1.5:1000
590 dilution). For the eIF2B5$^{R132H/R132H}$ studies, cerebrums were harvested from 7 and 10
591 month old mice and protein was extracted using a lysis buffer containing 1% triton,
592 0.5% NaDOC, 0.1% SDS, 50 mM Tris pH 8, 100 mM NaCl, 10 mM β-
593 glycerophosphate, 5 mM NaF, 1 mM DTT, 1 mM vanadate, and EDTA-free complete
594 TM protease inhibitor cocktail (#11-836-170-001; ROCHE). Protein was quantified

595 using a BCA protein assay kit (#23227 Pierce), diluted in 1X sample buffer (0.05 M
596 HEPES pH 7.4, 2% (w/v) SDS, 10% (v/v) Glycerol, traces of Bromophenol Blue, 100
597 mM Dithiothreitol (DTT)), and separated on a 10% SDS-PAGE gel. Blots were imaged
598 using an AI600 Imager (Amersham) and quantified by ImageQuant TL (GE
599 Healthcare, Pittsburgh, PA, United States).
600
601 **Behavioral studies**
602 **Animals included.** Subjects were *Mcl-1*$^{cKO}$ mice or littermate controls with intact Mcl-
603 1, including genotypes Mcl1$^{f/+}$ without Cre, Mcl1$^{f/f}$ without Cre, and Gfap-Cre/Mcl1$^{f/+}$.
604 A total of 8 litters were needed to generate all of the replicates. Day of birth was
605 considered postnatal day 0 (P0). Subject numbers at the beginning of the study (P7)
606 were 13 (21%) *Mcl-1*$^{cKO}$ and 48 (79%) control. All litters completed the first 2 weeks
607 of testing. Three litters (n=23) were removed from the study for histology assays
608 during the third week of testing: one on P15, after the second open field test; one on
609 PD16, after the first acoustic startle test; and one on P21, after the tail suspension
610 test.
611
612 **Behavioral testing regimen**
613 **Developmentally-calibrated behavioral tests:** For motor tests at P7, mice were
614 removed from the home cage and maintained in a beaker warmed to 35°C. Mice were
615 then subjected to the neurobehavioral negative geotaxis, righting, and open field
616 tests, adapted from published studies (Cheh et al., 2006).
617 **Negative geotaxis**. A 20 cm × 20 cm screen with 0.5 cm wire mesh squares was set
618 at a 25° angle. Each pup was placed downward on the screen with its head facing
619 toward the bottom, allowed to grip the mesh, and then released. The time it took for

620 each pup to turn 180° (head and upper torso vertical), was recorded, with a 30 s
621 maximum and each pup was tested 3 times.
622 **Righting.** Each pup was placed onto its back on a flat Plexiglas surface. The
623 experimenter gently held the pup in place for 2 s and then released it. The latency to
624 righting (all 4 feet on the ground) was timed, with a maximum of 30 s.
625 **Open field activity and pivoting.** Each pup was placed into the center of a Plexiglas
626 chamber (PhenoTyper; 30.5 cm × 30.5 cm × 43.5 cm; Noldus Information
627 Technology, Wageningen, The Netherlands). A dim yellow light (30 lx) at the top of
628 the PhenoTyper box was illuminated throughout the 3 min trial. Measures were taken
629 of distance traveled and time in the center region (4 cm × 4 cm square in the center
630 of the arena) by an image-tracking system (EthoVision, Noldus Information
631 Technology). In addition, the experimenter recorded the number of vertical rearing
632 movements and number of pivots (circling or lateral movement, as opposed to
633 forward locomotion).
634 Each mouse was screened through the 3 assays in the order presented here. After
635 finishing the neonatal motor screen, each pup was weighed, marked with a non-toxic
636 Sharpie, and placed back into the warm beaker. The litter was returned to the home
637 cage after all pups had been tested.
638
639 **Open field activity at P14 and P19.** Additional open field activity tests were
640 performed at P14 and P19. The distance traveled, the number of vertical rearing
641 movements, and time spent in the center region was recorded in each 10 min test.
642
643 **Acoustic startle responses.** This test was used to assess auditory function,
644 reactivity to environmental stimuli, and sensorimotor gating. Mice were evaluated at

645 2 time points, P14 and P21. The procedure was based on the reflexive whole-body
646 flinch, or startle response, that follows exposure to the acoustic stimuli. Measures
647 were taken of startle magnitude and prepulse inhibition, which occurs when a weak
648 stimulus leads to a reduced startle in response to a subsequent louder noise.

649 Mice were placed into individual Plexiglas cylinders within larger, sound-
650 attenuating chambers. Each cylinder was seated upon a piezoelectric transducer,
651 which allowed vibrations to be quantified and displayed on a computer (San Diego
652 Instruments SR-Lab system). The chambers included a ceiling light, fan, and a
653 loudspeaker for the acoustic stimuli. Background sound levels (70 dB) and calibration
654 of the acoustic stimuli were confirmed with a digital sound level meter (San Diego
655 Instruments). Each session began with a 5-min habituation period, followed by 42
656 trials of 7 different types: no-stimulus (NoS) trials, trials with the acoustic startle
657 stimulus (AS; 40 msec, 120 dB) alone, and trials in which a prepulse stimulus (20
658 msec; either 74, 78, 82, 86, or 90 dB) occurred 100 ms before the onset of the startle
659 stimulus. Measures were taken of the startle amplitude for each trial across a 65-
660 msec sampling window, and an overall analysis was performed for each subject's
661 data for levels of prepulse inhibition at each prepulse sound level (calculated as 100
662 - [(response amplitude for prepulse stimulus and startle stimulus together / response
663 amplitude for startle stimulus alone) x 100].

664

665 **Limb clasping.** At PD18-21, a subset of mice (n=39) was assessed for limb clasping
666 during a tail-suspension test. Each mouse was lifted by the base of the tail, and
667 suspended above cage bedding for 15 sec, with ventral (stomach) side facing the
668 experimenter. Response to tail suspension was coded using the following scoring
669 system:

670

671 Forepaw movement

672 -2 = paws are clasped together, little movement, may be drawn up against

673 chest

674 0 = paws move quickly in periodic flailing or kicking motions

675 2 = vigorous movement, may resemble rapid digging

676 Hindlimb placement and movement

677 -4 = both hindlimbs are retracted inwards toward abdomen, with little

678 movement

679 -2 = hindlimbs are partially or intermittently retracted inwards toward abdomen

680 0 = hindlimbs are splayed outward from the abdomen. Moderate kicking behavior

681 2 = vigorous rapid kicking

682

683 **Statistical analysis of behavioral tests**

684 All testing was conducted by experimenters blinded to mouse genotype. Statview

685 (SAS, Cary, NC) was used for data analyses. To reduce the number of *Mcl-1*$^{cKO}$

686 subjects required, behavioral data from males and females were combined. One-

687 way or repeated measures analysis of variance (ANOVA) were used to determine

688 effects of genotype. Post-hoc analyses were conducted using Fisher's Protected

689 Least Significant Difference (PLSD) tests following a significant ANOVA F value. For

690 all comparisons, significance was set at $p<0.05$.

691

692

693 **Supplementary Figures**

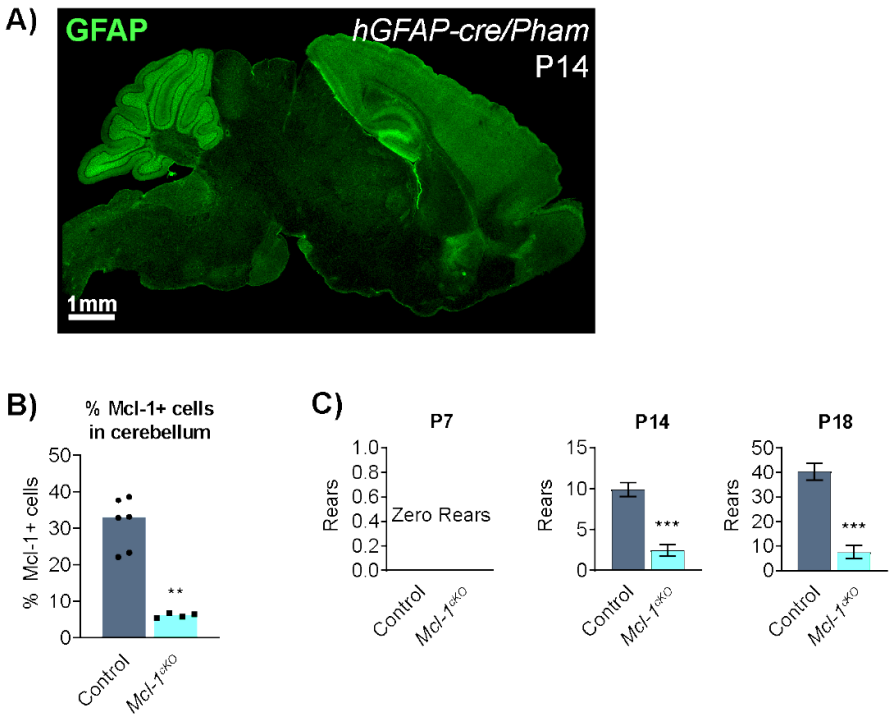


694

695 **Supplementary Figure 1. *hGFAP-Cre* conditionally deletes *Mcl-1* in regions**
696 **throughout the brain. A)** *hGFAP-Cre* induces expression of the fluorescent reporter
697 DENDRA2 in *hGFAP-cre/Pham* mice, indicating regions of GFAP expression. *hGFAP-*
698 *Cre* targets cells in diverse regions throughout the brain, including the cerebellum,
699 hippocampus, and cortex. **B)** MCL-1 protein levels are significantly reduced in
700 cerebella of *Mcl-1*$^{cKO}$ mice. **C)** *Mcl-1*$^{cKO}$ mice displayed decreased rearing at both P14
701 and P18.

702

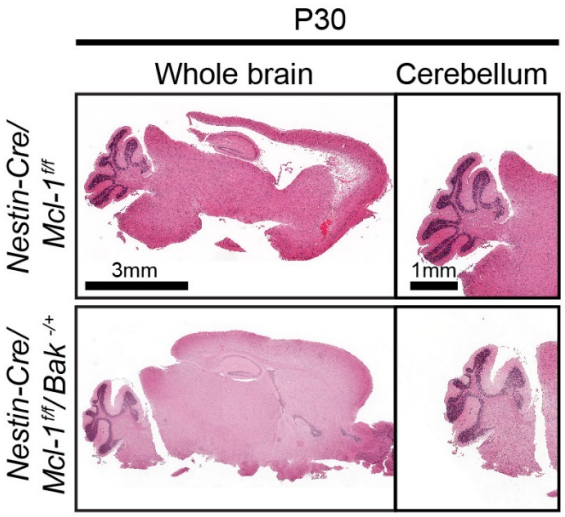


703

704 **Supplementary Figure 2. *Nestin-Cre/Mcl-1$^{f/f}$* mice develop white matter**
705 **degeneration similar to that of *Mcl-1$^{cKO}$* mice.** Similar to GFAP-Cre, Nestin-Cre
706 targets cells of both the neural and glial lineage. Brains harvested from *Nestin-*
707 *Cre/Mcl-1$^{f/f}$* mice showed ventricular dilation and white matter rarefaction by P30.
708 Deletion of one copy of *Bak* rescued this phenotype in *Nestin-Cre/Mcl-1$^{f/f}$/Bak$^{-/+}$* mice.

709

710

711 **References**


712 ABBINK, T. E. M., WISSE, L. E., JAKU, E., THIECKE, M. J., VOLTOLINI-GONZALEZ, D., FRITSEN,
713 H., BOBELDIJK, S., TER BRAAK, T. J., POLDER, E., POSTMA, N. L., BUGIANI, M.,
714 STRUIJS, E. A., VERHEIJEN, M., STRAAT, N., VAN DER SLUIS, S., THOMAS, A. A. M.,
715 MOLENAAR, D. & VAN DER KNAAP, M. S. 2019. Vanishing white matter: deregulated
716 integrated stress response as therapy target. *Ann Clin Transl Neurol,* 6**,** 1407-1422.
717 BUGIANI, M., BOOR, I., POWERS, J. M., SCHEPER, G. C. & VAN DER KNAAP, M. S. 2010.
718 Leukoencephalopathy with vanishing white matter: a review. *J Neuropathol Exp*
719 *Neurol,* 69**,** 987-96.
720 BUGIANI, M., BOOR, I., VAN KOLLENBURG, B., POSTMA, N., POLDER, E., VAN BERKEL, C.,
721 VAN KESTEREN, R. E., WINDREM, M. S., HOL, E. M., SCHEPER, G. C., GOLDMAN, S. A.
722 & VAN DER KNAAP, M. S. 2011. Defective glial maturation in vanishing white matter
723 disease. *J Neuropathol Exp Neurol,* 70**,** 69-82.
724 BUGIANI, M., POSTMA, N., POLDER, E., DIELEMAN, N., SCHEFFER, P. G., SIM, F. J., VAN DER
725 KNAAP, M. S. & BOOR, I. 2013. Hyaluronan accumulation and arrested
726 oligodendrocyte progenitor maturation in vanishing white matter disease. *Brain,*
727 136**,** 209-22.
728 BUGIANI, M., VUONG, C., BREUR, M. & VAN DER KNAAP, M. S. 2018. Vanishing white
729 matter: a leukodystrophy due to astrocytic dysfunction. *Brain Pathol,* 28**,** 408-421.
730 CHEH, M. A., MILLONIG, J. H., ROSELLI, L. M., MING, X., JACOBSEN, E., KAMDAR, S. &
731 WAGNER, G. C. 2006. En2 knockout mice display neurobehavioral and neurochemical
732 alterations relevant to autism spectrum disorder. *Brain Res,* 1116**,** 166-76.
733 CHONG, M. J., MURRAY, M. R., GOSINK, E. C., RUSSELL, H. R. C., SRINIVASAN, A., KAPSETAKI,
734 M., KORSMEYER, S. J. & MCKINNON, P. J. 2000. Atm and Bax cooperate in ionizing
735 radiation-induced apoptosis in the central nervous system. *Proceedings of the*
736 *National Academy of Sciences,* 97**,** 889-894.
737 CLARKE, S. R., SHETTY, A. K., BRADLEY, J. L. & TURNER, D. A. 1994. Reactive astrocytes
738 express the embryonic intermediate neurofilament nestin. *Neuroreport,* 5**,** 1885-8.
739 CROWTHER, A. J., GAMA, V., BEVILACQUA, A., CHANG, S. X., YUAN, H., DESHMUKH, M. &
740 GERSHON, T. R. 2013. Tonic activation of Bax primes neural progenitors for rapid
741 apoptosis through a mechanism preserved in medulloblastoma. *The Journal of*
742 *neuroscience : the official journal of the Society for Neuroscience,* 33**,** 18098-108.
743 CROWTHER, A. J., OCASIO, J. K., FANG, F., MEIDINGER, J., WU, J., DEAL, A. M., CHANG, S. X.,
744 YUAN, H., SCHMID, R., DAVIS, I. & GERSHON, T. R. 2016. Radiation Sensitivity in a
745 Preclinical Mouse Model of Medulloblastoma Relies on the Function of the Intrinsic
746 Apoptotic Pathway. *Cancer Res,* 76**,** 3211-23.
747 DAHL, D. & BIGNAMI, A. 1974. Heterogeneity of the glial fibrillary acidic protein in gliosed
748 human brains. *J Neurol Sci,* 23**,** 551-63.
749 DOOVES, S., BUGIANI, M., POSTMA, N. L., POLDER, E., LAND, N., HORAN, S. T., VAN DEIJK, A.
750 L., VAN DE KREEKE, A., JACOBS, G., VUONG, C., KLOOSTER, J., KAMERMANS, M.,
751 WORTEL, J., LOOS, M., WISSE, L. E., SCHEPER, G. C., ABBINK, T. E., HEINE, V. M. &
752 VAN DER KNAAP, M. S. 2016. Astrocytes are central in the pathomechanisms of
753 vanishing white matter. *J Clin Invest,* 126**,** 1512-24.
754 DZHAGALOV, I., ST JOHN, A. & HE, Y. W. 2007. The antiapoptotic protein Mcl-1 is essential
755 for the survival of neutrophils but not macrophages. *Blood,* 109**,** 1620-6.

EDDLESTON, M. & MUCKE, L. 1993. Molecular profile of reactive astrocytes--implications for their role in neurologic disease. *Neuroscience,* 54**,** 15-36.

ELROY-STEIN, O. 2017. Mitochondrial malfunction in vanishing white matter disease: a disease of the cytosolic translation machinery. *Neural Regen Res,* 12**,** 1610-1612.

FOGARTY, L. C., FLEMMER, R. T., GEIZER, B. A., LICURSI, M., KARUNANITHY, A., OPFERMAN, J. T., HIRASAWA, K. & VANDERLUIT, J. L. 2019. Mcl-1 and Bcl-xL are essential for survival of the developing nervous system. *Cell Death Differ,* 26**,** 1501-1515.

FOGLI, A., WONG, K., EYMARD-PIERRE, E., WENGER, J., BOUFFARD, J. P., GOLDIN, E., BLACK, D. N., BOESPFLUG-TANGUY, O. & SCHIFFMANN, R. 2002. Cree leukoencephalopathy and CACH/VWM disease are allelic at the EIF2B5 locus. *Ann Neurol,* 52**,** 506-10.

FRITSCH, R. M., SCHNEIDER, G., SAUR, D., SCHEIBEL, M. & SCHMID, R. M. 2007. Translational repression of MCL-1 couples stress-induced eIF2 alpha phosphorylation to mitochondrial apoptosis initiation. *J Biol Chem,* 282**,** 22551-62.

GEVA, M., CABILLY, Y., ASSAF, Y., MINDROUL, N., MAROM, L., RAINI, G., PINCHASI, D. & ELROY-STEIN, O. 2010. A mouse model for eukaryotic translation initiation factor 2B-leucodystrophy reveals abnormal development of brain white matter. *Brain,* 133**,** 2448-61.

GLASGOW, S. M., ZHU, W., STOLT, C. C., HUANG, T. W., CHEN, F., LOTURCO, J. J., NEUL, J. L., WEGNER, M., MOHILA, C. & DENEEN, B. 2014. Mutual antagonism between Sox10 and NFIA regulates diversification of glial lineages and glioma subtypes. *Nat Neurosci,* 17**,** 1322-9.

GUYENET, S. J., FURRER, S. A., DAMIAN, V. M., BAUGHAN, T. D., LA SPADA, A. R. & GARDEN, G. A. 2010. A simple composite phenotype scoring system for evaluating mouse models of cerebellar ataxia. *J Vis Exp*.

HASAN, S. M., SHEEN, A. D., POWER, A. M., LANGEVIN, L. M., XIONG, J., FURLONG, M., DAY, K., SCHUURMANS, C., OPFERMAN, J. T. & VANDERLUIT, J. L. 2013. Mcl1 regulates the terminal mitosis of neural precursor cells in the mammalian brain through p27Kip1. *Development,* 140**,** 3118-27.

HATTEN, M. E. 1990. Riding the glial monorail: a common mechanism for glial-guided neuronal migration in different regions of the developing mammalian brain. *Trends Neurosci,* 13**,** 179-84.

HERRERO, M., MANDELBOUM, S. & ELROY-STEIN, O. 2019. eIF2B Mutations Cause Mitochondrial Malfunction in Oligodendrocytes. *Neuromolecular Med,* 21**,** 303-313.

IMAI, Y., IBATA, I., ITO, D., OHSAWA, K. & KOHSAKA, S. 1996. A novel gene iba1 in the major histocompatibility complex class III region encoding an EF hand protein expressed in a monocytic lineage. *Biochem Biophys Res Commun,* 224**,** 855-62.

ITO, D., IMAI, Y., OHSAWA, K., NAKAJIMA, K., FUKUUCHI, Y. & KOHSAKA, S. 1998. Microglia-specific localisation of a novel calcium binding protein, Iba1. *Brain Res Mol Brain Res,* 57**,** 1-9.

KANTOR, L., HARDING, H. P., RON, D., SCHIFFMANN, R., KANESKI, C. R., KIMBALL, S. R. & ELROY-STEIN, O. 2005. Heightened stress response in primary fibroblasts expressing mutant eIF2B genes from CACH/VWM leukodystrophy patients. *Hum Genet,* 118**,** 99-106.

KOHLER, W., CURIEL, J. & VANDERVER, A. 2018. Adulthood leukodystrophies. *Nat Rev Neurol,* 14**,** 94-105.

KOHLSCHUTTER, A. & EICHLER, F. 2011. Childhood leukodystrophies: a clinical perspective. *Expert Rev Neurother,* 11**,** 1485-96.

803 KUANG, Y., LIU, Q., SHU, X., ZHANG, C., HUANG, N., LI, J., JIANG, M. & LI, H. 2012. Dicer1 and
804 MiR-9 are required for proper Notch1 signaling and the Bergmann glial phenotype in
805 the developing mouse cerebellum. *Glia,* 60**,** 1734-46.
806 LANG, P. Y., NANJANGUD, G. J., SOKOLSKY-PAPKOV, M., SHAW, C., HWANG, D., PARKER, J.
807 S., KABANOV, A. V. & GERSHON, T. R. 2016. ATR maintains chromosomal integrity
808 during postnatal cerebellar neurogenesis and is required for medulloblastoma
809 formation. *Development,* 143**,** 4038-4052.
810 LEEGWATER, P. A., VERMEULEN, G., KONST, A. A., NAIDU, S., MULDERS, J., VISSER, A.,
811 KERSBERGEN, P., MOBACH, D., FONDS, D., VAN BERKEL, C. G., LEMMERS, R. J.,
812 FRANTS, R. R., OUDEJANS, C. B., SCHUTGENS, R. B., PRONK, J. C. & VAN DER KNAAP,
813 M. S. 2001. Subunits of the translation initiation factor eIF2B are mutant in
814 leukoencephalopathy with vanishing white matter. *Nat Genet,* 29**,** 383-8.
815 MALONE, C. D., HASAN, S. M., ROOME, R. B., XIONG, J., FURLONG, M., OPFERMAN, J. T. &
816 VANDERLUIT, J. L. 2012. Mcl-1 regulates the survival of adult neural precursor cells.
817 *Mol Cell Neurosci,* 49**,** 439-47.
818 MELCHIONDA, L., HAACK, T. B., HARDY, S., ABBINK, T. E., FERNANDEZ-VIZARRA, E.,
819 LAMANTEA, E., MARCHET, S., MORANDI, L., MOGGIO, M., CARROZZO, R., TORRACO,
820 A., DIODATO, D., STROM, T. M., MEITINGER, T., TEKTURK, P., YAPICI, Z., AL-
821 MURSHEDI, F., STEVENS, R., RODENBURG, R. J., LAMPERTI, C., ARDISSONE, A.,
822 MORONI, I., UZIEL, G., PROKISCH, H., TAYLOR, R. W., BERTINI, E., VAN DER KNAAP,
823 M. S., GHEZZI, D. & ZEVIANI, M. 2014. Mutations in APOPT1, encoding a
824 mitochondrial protein, cause cavitating leukoencephalopathy with cytochrome c
825 oxidase deficiency. *Am J Hum Genet,* 95**,** 315-25.
826 NAKAMURA, A., SWAHARI, V., PLESTANT, C., SMITH, I., MCCOY, E., SMITH, S., MOY, S. S.,
827 ANTON, E. S. & DESHMUKH, M. 2016. Bcl-xL Is Essential for the Survival and Function
828 of Differentiated Neurons in the Cortex That Control Complex Behaviors. *J Neurosci,*
829 36**,** 5448-61.
830 NISHIYAMA, A., BOSHANS, L., GONCALVES, C. M., WEGRZYN, J. & PATEL, K. D. 2016. Lineage,
831 fate, and fate potential of NG2-glia. *Brain Res,* 1638**,** 116-128.
832 OCASIO, J. K., BATES, R. D. P., RAPP, C. D. & GERSHON, T. R. 2019. GSK-3 modulates SHH-
833 driven proliferation in postnatal cerebellar neurogenesis and medulloblastoma.
834 *Development,* 146.
835 RAINI, G., SHARET, R., HERRERO, M., ATZMON, A., SHENOY, A., GEIGER, T. & ELROY-STEIN,
836 O. 2017. Mutant eIF2B leads to impaired mitochondrial oxidative phosphorylation in
837 vanishing white matter disease. *J Neurochem,* 141**,** 694-707.
838 RAKIC, P. 1971. Neuron-glia relationship during granule cell migration in developing
839 cerebellar cortex. A Golgi and electronmicroscopic study in Macacus Rhesus. *J Comp*
840 *Neurol,* 141**,** 283-312.
841 RAYMOND, G. V. 2017. Leukodystrophy: Basic and Clinical. *Adv Neurobiol,* 15**,** 365-382.
842 SAHIN KAYA, S., MAHMOOD, A., LI, Y., YAVUZ, E. & CHOPP, M. 1999. Expression of nestin
843 after traumatic brain injury in rat brain. *Brain Res,* 840**,** 153-7.
844 SCHMIDT-KASTNER, R., AGUIRRE-CHEN, C., SAUL, I., YICK, L., HAMASAKI, D., BUSTO, R. &
845 GINSBERG, M. D. 2005. Astrocytes react to oligemia in the forebrain induced by
846 chronic bilateral common carotid artery occlusion in rats. *Brain Res,* 1052**,** 28-39.
847 TAMAGNO, I. & SCHIFFER, D. 2006. Nestin expression in reactive astrocytes of human
848 pathology. *J Neurooncol,* 80**,** 227-33.

849 TECH, K., TIKUNOV, A. P., FAROOQ, H., MORRISSY, A. S., MEIDINGER, J., FISH, T., GREEN, S.
850 C., LIU, H., LI, Y., MUNGALL, A. J., MOORE, R. A., MA, Y., JONES, S. J. M., MARRA, M.
851 A., VANDER HEIDEN, M. G., TAYLOR, M. D., MACDONALD, J. M. & GERSHON, T. R.
852 2017. Pyruvate Kinase Inhibits Proliferation during Postnatal Cerebellar
853 Neurogenesis and Suppresses Medulloblastoma Formation. *Cancer Res,* 77**,** 3217-
854 3230.
855 VAN DER KNAAP, M. S., BARTH, P. G., GABREELS, F. J., FRANZONI, E., BEGEER, J. H., STROINK,
856 H., ROTTEVEEL, J. J. & VALK, J. 1997. A new leukoencephalopathy with vanishing
857 white matter. *Neurology,* 48**,** 845-55.
858 VAN DER KNAAP, M. S. & BUGIANI, M. 2017. Leukodystrophies: a proposed classification
859 system based on pathological changes and pathogenetic mechanisms. *Acta*
860 *Neuropathol,* 134**,** 351-382.
861 VAN DER KNAAP, M. S. & BUGIANI, M. 2018. Leukodystrophies - much more than just
862 diseases of myelin. *Nat Rev Neurol,* 14**,** 747-748.
863 VAN DER KNAAP, M. S., FOGLI, A., BOESPFLUG-TANGUY, O., ABBINK, T. E. M. &
864 SCHIFFMANN, R. 1993. Childhood Ataxia with Central Nervous System
865 Hypomyelination / Vanishing White Matter. *In:* ADAM, M. P., ARDINGER, H. H.,
866 PAGON, R. A., WALLACE, S. E., BEAN, L. J. H., STEPHENS, K. & AMEMIYA, A. (eds.)
867 *GeneReviews((R)).* Seattle (WA).
868 VAN DER KNAAP, M. S., PRONK, J. C. & SCHEPER, G. C. 2006. Vanishing white matter disease.
869 *Lancet Neurol,* 5**,** 413-23.
870 VANDERVER, A., TONDUTI, D., SCHIFFMANN, R., SCHMIDT, J. & VAN DER KNAAP, M. S. 1993.
871 Leukodystrophy Overview - ARCHIVED CHAPTER, FOR HISTORICAL REFERENCE ONLY.
872 *In:* ADAM, M. P., ARDINGER, H. H., PAGON, R. A., WALLACE, S. E., BEAN, L. J. H.,
873 STEPHENS, K. & AMEMIYA, A. (eds.) *GeneReviews((R)).* Seattle (WA).
874 YASUDA, O., FUKUO, K., SUN, X., NISHITANI, M., YOTSUI, T., HIGUCHI, M., SUZUKI, T.,
875 RAKUGI, H., SMITHIES, O., MAEDA, N. & OGIHARA, T. 2006. Apop-1, a novel protein
876 inducing cyclophilin D-dependent but Bax/Bak-related channel-independent
877 apoptosis. *J Biol Chem,* 281**,** 23899-907.
878 ZHOU, L., LI, P., CHEN, N., DAI, L. F., GAO, K., LIU, Y. N., SHEN, L., WANG, J. M., JIANG, Y. W.
879 & WU, Y. 2019. Modeling vanishing white matter disease with patient-derived
880 induced pluripotent stem cells reveals astrocytic dysfunction. *CNS Neurosci Ther,* 25**,**
881 759-771.
882 ZHUO, L., THEIS, M., ALVAREZ-MAYA, I., BRENNER, M., WILLECKE, K. & MESSING, A. 2001.
883 hGFAP-cre transgenic mice for manipulation of glial and neuronal function in vivo.
884 *genesis,* 31**,** 85-94.
885

886

887

888

889

890

891